NIFS--137

JP9211231

Field Line Diversion Properties of Finite β Helias Equilibria

T. Hayashi, U. Schwenn and E. Strumberger

(Received – Feb. 14, 1992)

NIFS-137 Mar. 1992

FIELD LINE DIVERSION PROPERTIES OF FINITE β HELIAS EQUILIBRIA

T. Hayashi*, U. Schwenn, E. Strumberger

Max-Planck-Institut für Plasmaphysik
IPP-EURATOM Association, D-8046 Garching bei München

*National Institute for Fusion Science, Nagoya, Japan

Abstract

The diversion properties of the magnetic field outside the last closed magnetic surface of a Helias stellarator configuration [1] are investigated for finite β-equilibria. The results support a divertor concept which has been developed from the diversion properties of the *corresponding* vacuum field. Cross-field transport is simulated by a simplified scrape-off layer (SOL) model.

1. Introduction

In experiments such as Heliotron-E [2], ATF [3], and Wendelstein VII-AS [4] characteristic stripes along the torus wall have been observed that are due to plasma-wall interaction. The positions of these stripes correspond to those of the helical edges characteristic of Helias configurations [1]. In a Helias configuration with N periods N half-helix-like edges run along the toroidally outward side of the plasma boundary and afford the possibility of separatrix formation owing to the coincidence of the helical edge and x-points between islands. Fig. 1 shows the plasma tube and its five helical edges for the proposed Wendelstein 7-X stellarator [5].

By investigating the diversion properties of the vacuum magnetic field outside the last closed magnetic surface a divertor concept could be developed for W7-X [6]. Fig. 2 shows the plasma tube and the so-called 'helical troughs' which fulfill the following conditions:

- They do not act as limiters, but rather as divertor plates.
- They lead to a complete separation of the magnetic field lines starting at the plasma and ending at the divertor trough from the field lines starting at the first wall.
- This separation is independent of the detailed island positions.

Here, it is investigated whether this divertor concept is robust for finite β-equilibria. In section 2, the diversion properties of a vacuum field produced by an optimized coil system are reviewed. Then, in section 3, the magnetic field of a finite β-equilibrium, obtained by the HINT-code, and its corresponding vacuum field are compared, and the diversion properties of the finite β-equilibrium are studied. A summary of the results is given in section 4.

2. The vacuum magnetic field

The vacuum magnetic field, shown in Fig. 3, is obtained from an optimized coil configuration [7] which has a sufficiently large distance so that divertor equipment (dark blue areas) can be installed between the plasma and the cryostat (dashed line) containing the superconducting modular coils. The current-carrying surface belonging to this coil system is given by the outer black solid line. The last closed surface (green dotted line) lies

outside the five islands ($\iota = \frac{5}{5}$) (red dots) in this case, while outside the last closed flux surface there is an ergodic region where only remnants close to the fixed points of the ($\iota = \frac{10}{9}$) islands (blue dots) can be found.

In order to describe the space between the plasma surface and the outer current-carrying surface in an adequate manner, the coordinate system (s, u, v), defined in [6], is used. The coordinates u (poloidal) and v (toroidal) are angle-like variables ($0 \leq u, v < 1$), while s is a radial coordinate ($0 \leq s \leq 1$).

With a homogeneous distribution of points on a surface outside but very close to the plasma surface as starting points, magnetic field lines are traced in both directions. The field lines intersect the plasma facing surfaces of the helical troughs (see Fig. 4) under small angles, $(\Psi_{con}) \approx 4^{\circ}$. These relatively small values of the intersection angles are a consequence of the adequately chosen plasma facing surfaces of the helical troughs which are parts of a surface with fixed s-coordinate, the so-called control surface ($s_{con} = 0.2 \hat{=} \Delta_{pcs} \approx 0.1m$ for a device with $R_0 = 5.5m$, Δ_{pcs} = *distance plasma-control surface*), and which, therefore, incorporate the geometries of the last closed magnetic surface and the current-carrying surface. In Fig. 4 the helical troughs are marked by the hatched areas. Figure 4 again confirms that x-point regions in the ergodic region lying in the neighbourhood of a helical edge are positions where the field lines are diverted.

The intersection points form patterns on the plasma facing surfaces, shown in Fig. 5, whose details depend on the position of the helical troughs, but whose general structure - being close to the helical edge - originates from the island structure: islands and x-points are widest close to the edges. Furthermore, the intersection position depends on the direction of the magnetic field line. The red dots in Fig. 5 characterize the intersection points of the magnetic field lines surrounding the torus in negative direction, while the green ones represent the positive direction.

3. The finite β-equilibrium

The magnetic field of a finite β-equilibrium with an average β-value of $\langle\beta\rangle = 2.3\%$ was obtained by the HINT code [8] in a computational box. This code is used with a current distribution on a surface which lies completely outside the grid box. Therefore, a

current-carrying surface was used [9] which fulfills this condition and which produces approximately the same vacuum field as the coils used in the preceding section. The last closed flux surfaces of the two vacuum fields are compared in Fig. 6.

In Fig. 7 the vacuum magnetic field inside the grid box is shown, as obtained by the field line tracing part of the HINT-code. Again five small islands (red dots) lie inside the last closed surface (green dashed line).

In the case of the finite β-equilibrium the boundary region of the vacuum magnetic field is ergodized so that the five islands now lie in the ergodic region as it is shown in Fig. 8. Now, the last closed surface lies inside the five islands and the islands are partially ergodized.

Thus, the aspect ratio is larger for $\langle\beta\rangle = 2.3\%$. The positions of the helical edges and of the islands do not vary significantly (see Fig. 9). This behaviour is an important condition for a successful divertor operation. It guarantees that the field line diversion occurs in the same regions as in the vacuum case. The plasma boundary of the finite β-equilibrium lies completely inside the last closed surface of the vacuum field. This is a consequence of the very small radial shift of free-boundary Helias equilibria. The distance between plasma boundary and divertor troughs increases.

For the $\langle\beta\rangle = 2.3\%$ equilibrium the boundary field lines are traced until they intersect the plasma facing surfaces of the helical troughs. Fig. 10 shows the intersection pattern, while Fig. 11 represents the Poincaré plots of the boundary field lines. Again the intersection points are concentrated close to the helical edge on the divertor plates, and the two directions of the magnetic field lines can be distinguished, but the intersection pattern is more concentrated than in the vacuum case.

Finally, particle diffusion is taken into account. As in Ref. [6] an anomalous diffusion coefficient of $D = 1\frac{m^2}{s}$ is simulated in a simplified scrape-off layer (SOL) model. The diffusion is simulated by 'diffusion of field lines' obtained with random displacements during the field line tracing after characteristic mean free paths ($\lambda \approx 1m$). These calculations again confirm that the diversion process persists at the helical edge, that the detailed island structure is blurred (see Fig. 12), and that the interaction area on the helical troughs increases (see Fig. 13).

Due to the relatively small size of the grid box some of the traced field lines reach the boundary of this grid box before they intersect the plasma facing surfaces. Therefore, the

intersection patterns, shown in Fig. 10 and Fig. 13, are not quite complete. The results will not change significantly, if the size of the box is increased.

4. Summary

The calculations presented above confirm that the finite β-equilibrium shows the same diversion properties as the vacuum magnetic field. Since the positions of the helical edges are almost the same, the helical troughs defined for the vacuum magnetic field work as well in the case of the finite β-equilibrium.

The intersection pattern corresponding to the $\langle\beta\rangle = 2.3\%$ is more concentrated than for the vacuum field, and there is larger distance between the plasma boundary and the divertor troughs. This increase in distance is mainly due to the fact that - in the vacuum field - the $\frac{5}{5}$ islands lie in the region of nested surfaces. In further investigations a vacuum magnetic field will be used whose five islands already lie outside the last closed surface. Further calculations will also use a larger grid box.

Acknowledgements

The authors are most grateful to P. Merkel for providing the current distribution and to J. Nührenberg for many fruitful discussions. This work was done while one of the authors (T.H.) was visiting the IPP.

REFERENCES

[1] NÜHRENBERG, J., ZILLE, R., Phys. Letters **A 114** (1986) 129, Phys. Letters **A 129** (1988) 113.

[2] HILLIS, D.L., MIODUSZEWSKI, P.K., FOWLER, R.H. et al., J. Nucl. Mater. 162-164 (1989) 629.

[3] MIODUSZEWSKI, P.K., UCKAN, T., HILLIS, D.L. et. al., Proc. 16th Europ. Conf. on Contr. Fusion and Plasma Physics, Venice 1989, ECA, **13B**, part II, 623.

[4] BEIDLER, C., HARMEYER, E., KIBLINGER, J., RAU, F., WOBIG, H., W VII-AS TEAM, Proc. 17th. Europ. Conf. on Contr. Fusion and Plasma Heating, Amsterdam 1990, ECA, **14B**, part II, 517.

[5] GRIEGER, G., BEIDLER, C., HARMEYER, E. et al., Proc. 13th Int. Conf. on Plasma Physics and Contr. Nuclear Fusion Res., Washington 1990, paper IAEA-CN-53/G-1-6, for more details see: WENDELSTEIN 7-X, Application for Preferential Support, WENDELSTEIN Project Group, IPP-EURATOM Association, August 1990.

[6] STRUMBERGER, E., Proc. 18th. Europ. Conf. on Contr. Fusion and Plasma Physics, Berlin 1991, ECA, **15C**, part II, 173, and Nucl. Fusion (1992) to be published.

[7] MERKEL, P., Proc. 18th. Europ. Conf. on Contr. Fusion and Plasma Physics, Berlin 1991, ECA, **15C**, part II, 185, Eighth International Workshop on Stellarators, IAEA TC Meeting, Kharkov 1991, XVI-0-1.

[8] HARAFUJI, K., HAYASHI, T., SATO, T., J. Comp. Phys. **81** (1989) 169.

[9] MERKEL, P., private communication.

Figure captions

Fig. 1: Plasma tube with five helical edges marked by red lines.

Fig. 2: Plasma tube and helical troughs.

Fig. 3: Poincaré plots of the vacuum magnetic field for an optimized coil system. The outer black line describes the current-carrying surface. The dashed curve marks the first wall and the dark blue areas show the helical troughs. The red points represent the five islands lying inside the last closed surface which is given in green, while the nine islands belonging to $\iota = \frac{10}{9}$ are marked by blue dots.

Fig. 4: Poincaré plots of the traced magnetic field lines. The inner solid curve represents the plasma surface, while the outer one shows the current-carrying surface. The dashed curve marks the first wall and the hatched areas show the helical troughs.

Fig. 5: Intersection pattern in u, v-coordinates for a vacuum magnetic field. The red and green points mark the two directions of the magnetic field lines (green = positive, red = negative). The yellow areas represent the plasma facing surface of the helical troughs. The distance between the plasma and these troughs is $\approx$20% of the plasma radius.

Fig. 6: The inner black and red curves represent last closed surfaces of vacuum magnetic fields. The last closed surface shown in red belongs to a magnetic field, defined on a grid, which was calculated from a current-carrying surface outside the grid box marked by the pink frame. The plasma boundary represented by the inner black curve is determined from an optimized coil set. The corresponding current-carrying surface is marked by the outer black solid curve. The dashed curve represents the first wall and the blue area marks the position of the divertor trough.

Fig. 7: Poincaré plot of the vacuum magnetic field (HINT code). The red points represent the five islands lying inside the last closed surface which is given by the green points.

Fig. 8: Poincaré plot of the magnetic field for $\langle\beta\rangle = 2.3\%$. The plasma boundary (green points) lies inside the five islands.

Fig. 9: Comparison of plasma boundaries for $\langle\beta\rangle = 0$ (blue points) and $\langle\beta\rangle = 2.3\%$ (green points). The red points mark the five islands of the vacuum field, while the black points represent the last surface of the vacuum field inside the five islands.

Fig. 10: Intersection pattern for $\langle\beta\rangle = 2.3\%$. The yellow area represents the plasma facing surfaces of the helical troughs. The red and green points mark the two directions fo the magnetic field lines (red = negative, green = positive).

Fig. 11: Poincaré plot of the edge field lines for $\langle\beta\rangle = 2.3\%$.

Fig. 12: Poincaré plot of the edge field lines taking diffusion ($D = 1\frac{m^2}{s}$) into account.

Fig. 13: The same as in Fig. 10, but with diffusion $D = 1\frac{m^2}{s}$.

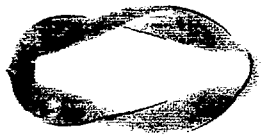

Fig. 1

Fig. 2

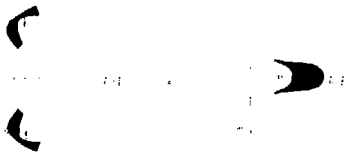

Fig. 3

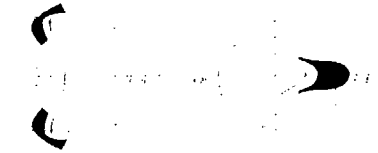

Fig. 6

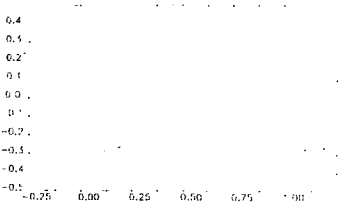

Fig. 5

Fig. 7

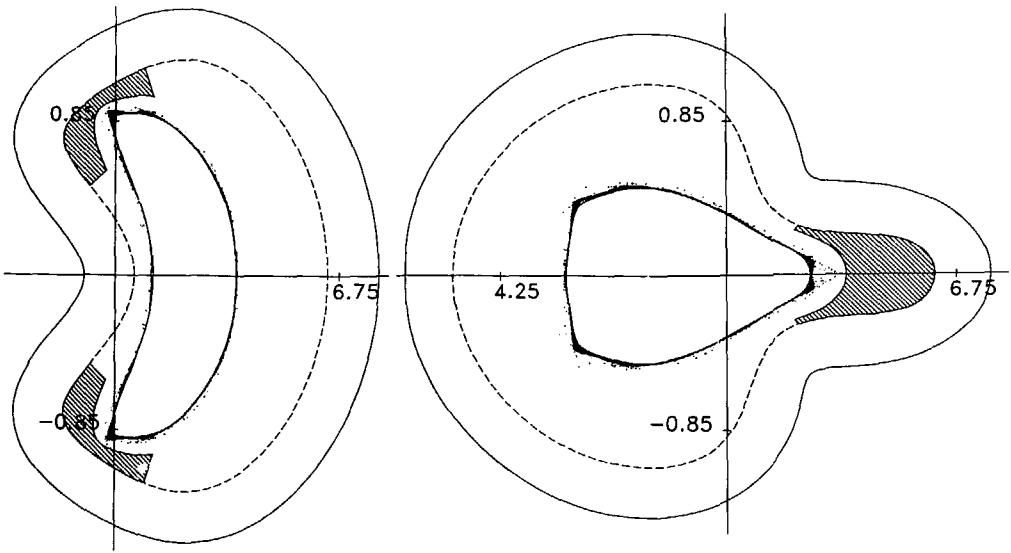

Fig. 4

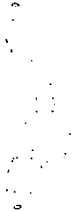

Fig. 8

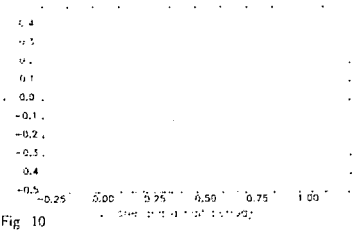

Fig. 10

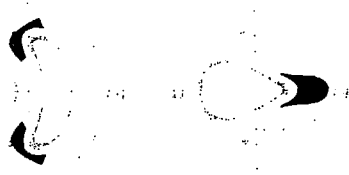

Fig. 12

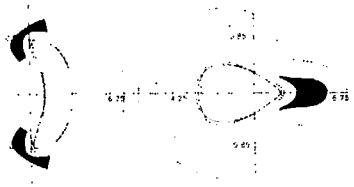

Fig. 9

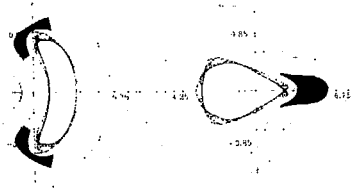

Fig. 11

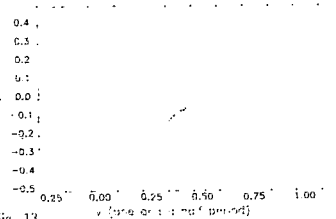

Fig. 13

Recent Issues of NIFS Series

NIFS-87 S. -I. Itoh, K. Itoh, A. Fukuyama, Y. Miura and JFT-2M Group, *ELMy-H mode as Limit Cycle and Chaotic Oscillations in Tokamak Plasmas;* May 1991

NIFS-88 N.Matsunami and K.Kitoh, *High Resolution Spectroscopy of H^+ Energy Loss in Thin Carbon Film;* May 1991

NIFS-89 H. Sugama, N. Nakajima and M.Wakatani, *Nonlinear Behavior of Multiple-Helicity Resistive Interchange Modes near Marginally Stable States;* May 1991

NIFS-90 H. Hojo and T.Hatori, *Radial Transport Induced by Rotating RF Fields and Breakdown of Intrinsic Ambipolarity in a Magnetic Mirror;* May 1991

NIFS-91 M. Tanaka, S. Murakami, H. Takamaru and T.Sato, *Macroscale Implicit, Electromagnetic Particle Simulation of Inhomogeneous and Magnetized Plasmas in Multi-Dimensions;* May 1991

NIFS-92 S. - I. Itoh, *H-mode Physics, -Experimental Observations and Model Theories-, Lecture Notes, Spring College on Plasma Physics, May 27 - June 21 1991 at International Centre for Theoretical Physics (IAEA UNESCO) Trieste, Italy ;* Jun. 1991

NIFS-93 Y. Miura, K. Itoh, S. - I. Itoh, T. Takizuka, H. Tamai, T. Matsuda, N. Suzuki, M. Mori, H. Maeda and O. Kardaun, *Geometric Dependence of the Scaling Law on the Energy Confinement Time in H-mode Discharges;* Jun. 1991

NIFS-94 H. Sanuki, K. Itoh, K. Ida and S. - I. Itoh, *On Radial Electric Field Structure in CHS Torsatron / Heliotron;* Jun. 1991

NIFS-95 K. Itoh, H. Sanuki and S I. Itoh, *Influence of Fast Ion Loss on Radial Electric Field in Wendelstein VII-A Stellarator;* Jun. 1991

NIFS-96 S. - I. Itoh, K. Itoh, A. Fukuyama, *ELMy-H mode as Limit Cycle and Chaotic Oscillations in Tokamak Plasmas;* Jun. 1991

NIFS-97 K. Itoh, S. - I. Itoh, H. Sanuki, A. Fukuyama, *An H-mode-Like Bifurcation in Core Plasma of Stellarators;* Jun. 1991

NIFS-98 H. Hojo, T. Watanabe, M. Inutake, M. Ichimura and S. Miyoshi, *Axial Pressure Profile Effects on Flute Interchange Stability in the Tandem Mirror GAMMA 10;* Jun. 1991

NIFS-99 A. Usadi, A. Kageyama, K. Watanabe and T. Sato, *A Global Simulation of the Magnetosphere with a Long Tail : Southward and Northward IMF;* Jun. 1991

NIFS-100 H. Hojo, T. Ogawa and M. Kono, *Fluid Description of Ponderomotive Force Compatible with the Kinetic One in a Warm Plasma* ; July 1991

NIFS-101 H. Momota, A. Ishida, Y. Kohzaki, G. H. Miley, S. Ohi, M. Ohnishi K. Yoshikawa, K. Sato, L. C. Steinhauer, Y. Tomita and M. Tuszewski *Conceptual Design of D-^{3}He FRC Reactor "ARTEMIS"* ; July 1991

NIFS-102 N. Nakajima and M. Okamoto, *Rotations of Bulk Ions and Impurities in Non-Axisymmetric Toroidal Systems* ; July 1991

NIFS-103 A. J. Lichtenberg, K. Itoh, S. - I. Itoh and A. Fukuyama, *The Role of Stochasticity in Sawtooth Oscillation* ; Aug. 1991

NIFS-104 K. Yamazaki and T. Amano, *Plasma Transport Simulation Modeling for Helical Confinement Systems;* Aug. 1991

NIFS-105 T. Sato, T. Hayashi, K. Watanabe, R. Horiuchi, M. Tanaka, N. Sawairi and K. Kusano, *Role of Compressibility on Driven Magnetic Reconnection ;* Aug. 1991

NIFS-106 Qian Wen - Jia, Duan Yun - Bo, Wang Rong - Long and H. Narumi, *Electron Impact Excitation of Positive Ions - Partial Wave Approach in Coulomb - Eikonal Approximation* ; Sep. 1991

NIFS-107 S. Murakami and T. Sato, *Macroscale Particle Simulation of Externally Driven Magnetic Reconnection;* Sep. 1991

NIFS-108 Y. Ogawa, T. Amano, N. Nakajima, Y. Ohyabu, K. Yamazaki, S. P. Hirshman, W. I. van Rij and K. C. Shaing, *Neoclassical Transport Analysis in the Banana Regime on Large Helical Device (LHD) with the DKES Code;* Sep. 1991

NIFS-109 Y. Kondoh, *Thought Analysis on Relaxation and General Principle to Find Relaxed State;* Sep. 1991

NIFS-110 H. Yamada, K. Ida, H. Iguchi, K. Hanatani, S. Morita, O. Kaneko, H. C. Howe, S. P. Hirshman, D. K. Lee, H. Arimoto, M. Hosokawa, H. Idei, S. Kubo, K. Matsuoka, K. Nishimura, S. Okamura, Y. Takeiri, Y. Takita and C. Takahashi, *Shafranov Shift in Low-Aspect-Ratio Heliotron / Torsatron CHS* ; Sep 1991

NIFS-111 R. Horiuchi, M. Uchida and T. Sato, *Simulation Study of Stepwise*

Relaxation in a Spheromak Plasma : Oct. 1991

NIFS-112 M. Sasao, Y. Okabe, A. Fujisawa, H. Iguchi, J. Fujita, H. Yamaoka and M. Wada, *Development of Negative Heavy Ion Sources for Plasma Potential Measurement* ; Oct. 1991

NIFS-113 S. Kawata and H. Nakashima, *Tritium Content of a DT Pellet in Inertial Confinement Fusion* ; Oct. 1991

NIFS-114 M. Okamoto, N. Nakajima and H. Sugama, *Plasma Parameter Estimations for the Large Helical Device Based on the Gyro-Reduced Bohm Scaling* ; Oct. 1991

NIFS-115 Y. Okabe, *Study of Au^- Production in a Plasma-Sputter Type Negative Ion Source* ; Oct. 1991

NIFS-116 M. Sakamoto, K. N. Sato, Y. Ogawa, K. Kawahata, S. Hirokura, S. Okajima, K. Adati, Y. Hamada, S. Hidekuma, K. Ida, Y. Kawasumi, M. Kojima, K. Masai, S. Morita, H. Takahashi, Y. Taniguchi, K. Toi and T. Tsuzuki, *Fast Cooling Phenomena with Ice Pellet Injection in the JIPP T-IIU Tokamak;* Oct. 1991

NIFS-117 K. Itoh, H. Sanuki and S. -I. Itoh, *Fast Ion Loss and Radial Electric Field in Wendelstein VII-A Stellarator;* Oct. 1991

NIFS-118 Y. Kondoh and Y. Hosaka, *Kernel Optimum Nearly-analytical Discretization (KOND) Method Applied to Parabolic Equations <<KOND-P Scheme>>;* Nov. 1991

NIFS-119 T. Yabe and T. Ishikawa, *Two- and Three-Dimensional Simulation Code for Radiation-Hydrodynamics in ICF*; Nov. 1991

NIFS-120 S. Kawata, M. Shiromoto and T. Teramoto, *Density-Carrying Particle Method for Fluid* ; Nov. 1991

NIFS-121 T. Ishikawa, P. Y. Wang, K. Wakui and T. Yabe, *A Method for the High-speed Generation of Random Numbers with Arbitrary Distributions;* Nov. 1991

NIFS-122 K. Yamazaki, H. Kaneko, Y. Taniguchi, O. Motojima and LHD Design *Group, Status of LHD Control System Design ; Dec. 1991*

NIFS-123 Y. Kondoh, *Relaxed State of Energy in Incompressible Fluid and Incompressible MHD Fluid* ; Dec. 1991

NIFS-124 K. Ida, S. Hidekuma, M. Kojima, Y. Miura, S. Tsuji, K. Hoshino, M.

Mori, N. Suzuki, T. Yamauchi and JFT-2M Group, *Edge Poloidal Rotation Profiles of H-Mode Plasmas in the JFT-2M Tokamak* ; Dec. 1991

NIFS-125 H. Sugama and M. Wakatani, *Statistical Analysis of Anomalous Transport in Resistive Interchange Turbulence* ;Dec. 1991

NIFS-126 K. Narihara, *A Steady State Tokamak Operation by Use of Magnetic Monopoles* ; Dec. 1991

NIFS-127 K. Itoh, S. -I. Itoh and A. Fukuyama, *Energy Transport in the Steady State Plasma Sustained by DC Helicity Current Drive* ;Jan. 1992

NIFS-128 Y. Hamada, Y. Kawasumi, K. Masai, H. Iguchi, A. Fujisawa, JIPP T-IIU Group and Y. Abe, *New High Voltage Parallel Plate Analyzer* ; Jan. 1992

NIFS-129 K. Ida and T. Kato, *Line-Emission Cross Sections for the Charge-exchange Reaction between Fully Stripped Carbon and Atomic Hydrogen in Tokamak Plasma*; Jan. 1992

NIFS-130 T. Hayashi, A. Takei and T. Sato, *Magnetic Surface Breaking in 3D MHD Equilibria of l=2 Heliotron* ; Jan. 1992

NIFS-131 K. Itoh, K. Iguchi and S. -I. Itoh, *Beta Limit of Resistive Plasma in Torsatron/Heliotron* ; Feb. 1992

NIFS-132 K. Sato and F. Miyawaki, *Formation of Presheath and Current-Free Double Layer in a Two-Electron-Temperture Plasma* ; Feb. 1992

NIFS-133 T. Maruyama and S. Kawata, *Superposed-Laser Electron Acceleration* Feb. 1992

NIFS-134 Y. Miura, F. Okano, N. Suzuki, M. Mori, K. Hoshino, H. Maeda, T. Takizuka, JFT-2M Group, S.-I. Itoh and K. Itoh, *Rapid Change of Hydrogen Neutral Energy Distribution at L/H-Transition in JFT-2M H-mode* ; Feb. 1992

NIFS-135 H. Ji, H. Toyama, A. Fujisawa, S. Shinohara and K. Miyamoto *Fluctuation and Edge Current Sustainment in a Reversed-Field-Pinch;* Feb. 1992

NIFS-136 K. Sato and F. Miyawaki, *Heat Flow of a Two-Electron Temperature Plasma through the Sheath in the Presence of Electron Emission* ; Mar. 1992